Mon. Not. R. Astron. Soc. **000**, 000–000 (0000) Printed 1 February 2008 (MN LATEX style file v1.4)

Cyclo–synchrotron emission from magnetically dominated active regions above accretion discs

T. Di Matteo[1], A. Celotti[2] and A. C. Fabian[1]
[1] *Institute of Astronomy, Madingley Road, Cambridge, CB3 OHA*
[2] *S.I.S.S.A., via Beirut 2–4, 34014 Trieste, Italy*

1 February 2008

ABSTRACT
We discuss the role of thermal cyclo–synchrotron emission in a magnetically dominated corona above an accretion disk in an active galaxy or a galactic black hole candidate. The dissipation occurs in localized active regions around the central black hole. Cyclo–synchrotron radiation is found to be an important process. In the case of galactic black hole candidates, its emission can dominate the inverse Compton scattering of the soft photon field produced by the disc by thermal electrons. We discuss observational predictions and the detectability of cyclo-synchrotron radiation both for these sources and radio-quiet active galactic nuclei.

Key words: radiation mechanisms - magnetic fields - galaxies: active - binaries: general - accretion discs

1 INTRODUCTION

Accretion onto a massive black hole is believed to provide the primary energy source in active galaxies (AGN) and in some galactic X-ray binaries (galactic black hole candidates, GBHC). It is still unclear which fraction of the energy is released radiatively in an accretion disk around the black hole compared to that dissipated in a tenuous hot plasma (corona) above it. Such dissipation probably occurs through release of magnetic energy expelled from the disk by buoyancy effects.

Strong support for this picture comes from the interpretation of high energy emission (from UV to γ–rays). Both the spectral characteristics, including reflection components, and the energetics are better explained within the context of disk-corona models (Haardt & Maraschi 1993). These assume the presence of a corona, the hot thermal electrons of which Compton scatter the soft photon field produced by, and self-consistently reprocessed in, the cold underlying disk. The observations of the ratios of UV and X-ray luminosities in different objects require that the hot plasma covering factor is less than unity, suggesting that the dissipation is localized in discrete emitting regions (Galeev, Rosner & Vaiana 1979; Haardt, Maraschi & Ghisellini 1994; Stern et al. 1995).

Within this framework we assume that the disk dissipates internally a fraction $(1-f)$ of the accretion power, $\eta L_{\rm Edd}$, while the remaining fraction f is stored in magnetic field structures which generate localized active regions. Given that here the energy is transferred via the magnetic field, we expect it to be at least in equipartition with the local radiation energy density. The magnetic field in such regions is given by $B^2/8\pi = f\eta L_{\rm Edd}/N4\pi(r_{\rm blob}R_{\rm s})^2c$, where N is the number of active regions at any time, $L_{\rm Edd}$ is the Eddington luminosity and $r_{\rm blob}$ is their typical size in units of the Schwarzschild radius, $R_{\rm s}$. This corresponds to a field of the order of

$$B = 3\times10^5\left(\frac{f\eta}{N}\right)^{1/2} r_{\rm blob}^{-1}\left(\frac{M}{10^6\,{\rm M}_\odot}\right)^{-1/2}\quad {\rm G}, \qquad (1)$$

where M is the black hole mass. Energetic electrons embedded in such a field radiate by cyclo-synchrotron (hereafter CS) emission. As we show in the following sections, under the temperature and density conditions required by the disk-corona models, the CS radiation is partially self-absorbed. However, this process can still significantly contribute to the cooling of the hot plasma. Indeed, CS emission has been shown to be relevant in the case of some GBHC (Cyg X-1 and GX339-4) and to explain the observed rapid optical variability in GX339-4 (Fabian et al. 1982; Apparao 1984).

Self–absorbed CS emission has also been previously considered in the context of accretion discs (Ipser & Price 1982, Zdziarski 1986 and references therein), while its contribution has often been neglected in the context of localized magnetically dominated active regions in a corona (e.g. Haardt et al. 1994). In this paper we derive a useful diagnostic in this specific context.

In particular, we examine in some detail the role of CS radiation losses in terms of both the electron cooling and the expected radiative signatures in AGN and GBHC. In

section 2 we estimate the CS cooling timescale and compare it to the inverse Compton one. The emitted spectrum and the possibility of detecting the CS radiation are discussed in section 3. Section 4 summarizes our conclusions.

2 CYCLO-SYNCHROTRON COOLING

In a thermal plasma, optically–thin synchrotron emission rises steeply with decreasing frequency. Under most circumstances the emission becomes self-absorbed and gives rise to a black-body spectrum below a critical frequency $\nu_{\rm c}$. Above this frequency it decays exponentially as expected from a thermal plasma, due to the superposition of cyclotron harmonics. The total cooling rate can be therefore estimated by taking into account the blackbody emission up to a frequency $\nu_{\rm c}$ and the CS one above $\nu_{\rm c}$. We show here that the inclusion of this latter component is important and can even exceed the emission from the optically thick part.

In a plasma with electron density n and dimensionless electron temperature $\theta = kT/m_{\rm e}c^2$, embedded in a magnetic field of strength B, the CS emissivity in the optically thin limit is given by (e.g. Pacholczyk 1970; Takahara & Tsuruta 1982)

$$\epsilon_\nu = 5.57 \times 10^{-29} \, \frac{n\nu I'(x)}{K_2(1/\theta)} \quad {\rm erg\,cm^{-3}\,s^{-1}\,Hz^{-1}}, \tag{2}$$

where $x \equiv 2\nu/3\nu_0\theta^2$, $\nu_0 = eB/2\pi m_{\rm e}c$, $K_2(1/\theta)$ is the modified Bessel function and $I'(x)$ is expressed as the average over all angles (with respect to the direction of B) for a mildly relativistic plasma with an isotropic velocity distribution. It can be approximated as (Mahadevan et al. 1996)

$$I'(x) = \frac{4.050}{x^{1/6}} \left(1 + \frac{0.40}{x^{1/4}} + \frac{0.532}{x^{1/2}}\right) \exp(-1.889 x^{1/3}). \tag{3}$$

The self-absorption frequency $\nu_{\rm c}$ is given by

$$\nu_{\rm c} = \frac{3}{2}\nu_0\theta^2 x_{\rm m}, \tag{4}$$

where $x_{\rm m}(\tau/B,\theta) \equiv x(\nu_{\rm c})$, can be determined by equating the CS emission (eqn. 2) to the Rayleigh-Jeans blackbody emission from the surface of a sphere of radius $r_{\rm blob}R_{\rm s}$, namely

$$\epsilon_\nu \frac{4\pi}{3}(r_{\rm blob}R_{\rm s})^3 = 8\pi^2 m_{\rm e}\nu^2\theta(r_{\rm blob}R_{\rm s})^2. \tag{5}$$

The cooling rate for the optically thin CS component, $\Lambda_{\rm thin}$, is determined by integrating ϵ_ν over frequencies above $\nu_{\rm c}$, while in the optically thick limit the cooling rate can be approximated by $\Lambda_{\rm thick} \approx (2\pi/3) m_{\rm e}\theta\nu_{\rm c}^3/r_{\rm blob}R_{\rm s}$. Fig. 1 shows the ratio of the two cooling rates ($\Lambda_{\rm thin}/\Lambda_{\rm thick}$) for different values of the plasma temperature θ and the Thomson optical depth $\tau = \sigma_{\rm T} n r_{\rm blob} R_{\rm s}$. As Fig. 1 illustrates, $\Lambda_{\rm thin}$ is comparable to $\Lambda_{\rm thick}$ and for $\theta \gtrsim 0.7$ it becomes the dominant cooling component. It therefore needs to be taken into account when calculating the cooling timescales for CS emission.

2.1 Cooling timescales

In order to establish the importance of typical CS losses in an active region, here we estimate the timescales for CS and Compton emission. The CS cooling timescale, $t_{\rm CS} \simeq nm_{\rm e}c^2\theta/(\Lambda_{\rm thick} + \Lambda_{\rm thin})$, is given by

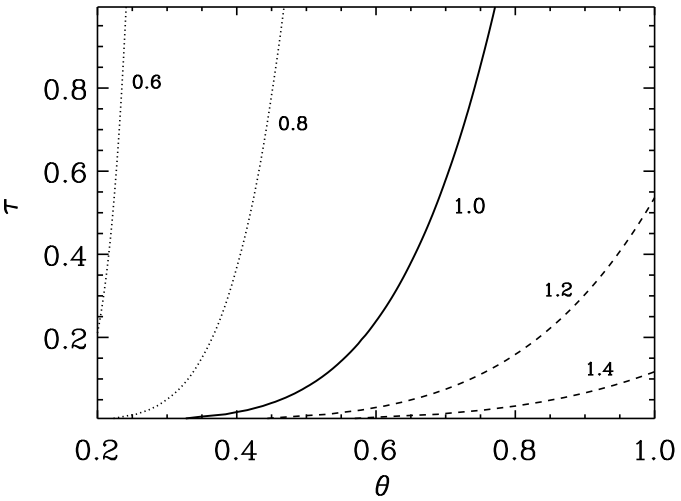

Figure 1. The plot represents the ratio $\Lambda_{\rm thin}/\Lambda_{\rm thick}$ as a function of θ and τ for CS emission for a typical GBHC. Curves are labelled with the respective values of this ratio.

$$t_{\rm CS} = \frac{3c^2}{2\pi\sigma_{\rm T}} \frac{\tau}{\Delta\nu_{\rm c}^3}. \tag{6}$$

where $\Delta = \Lambda_{\rm thick} + \Lambda_{\rm thin}$, the total cooling rate. By substituting $\nu_{\rm c}$, we obtain

$$t_{\rm CS} \simeq \frac{8.7 \times 10^{24}\tau}{\Delta B^3\theta^6 x_{\rm m}^3} \simeq \frac{0.3}{\Delta}\left(\frac{NM}{\eta f}\right)^{3/2} \frac{r_{\rm blob}^3\tau}{\theta^6 x_{\rm m}^3} \ {\rm s}. \tag{7}$$

$x_{\rm m}(\tau/B,\theta)$ is obtained by solving eqn. (5) and is plotted as a function of τ/B in Fig. 2.

$t_{\rm CS}$ can be compared with the timescale for inverse Compton cooling on the radiation field of the disk-photons

$$t_{\rm iC} = \frac{m_{\rm e}c}{4\sigma_{\rm T}} \frac{1}{U_{\rm rad}} = 2.7 \times 10^{-9} \frac{r_{\rm cor}^2 M}{\eta(1-f)} \quad {\rm s}, \tag{8}$$

where $U_{\rm rad} = (1-f)\eta L_{\rm Edd}/4\pi(r_{\rm cor}R_{\rm s})^2 c$ and $r_{\rm cor}$ is the total extent of the disc emission in units of $R_{\rm s}$.

In order to compare these timescales we choose appropriate ranges for the parameters τ and θ. As mentioned above, according to the 'standard' models for high energy emission, X-rays are due to Compton scattering of the soft photons by mildly–relativistic thermal electrons. For Seyfert galaxies, the canonical (intrinsic) X–ray spectral slope observed in AGN is of the order of $\alpha \simeq 1$, when the effect of reflection onto the thick accretion disk is taken into account. This spectral index and the typical energies of the high energy (γ–ray) cut–offs (e.g. Gondek et al. 1996) suggest a scattering plasma with $\tau \lesssim 0.5$. However, recent results (Poutanen et al. 1997, Zdziarski et al. 1997) derive values of $\tau \approx 1$ and electron temperatures $\approx 100\,{\rm keV}$. The quantitative relation between θ and τ and the energy spectral index α, for optically–thin plasmas, is given by $\alpha \simeq -\ln P/\ln(1 + 4\theta + 16\theta^2)$ where P is the average scattering probability $P = 1 + \exp(-\tau)/2\left(\tau^{-1} - 1\right) - 2\tau^{-1} + (\tau/2)E_1(\tau)$, and E_1 the exponential integral (Zdziarski et al. 1994). This scattering probability is calculated strictly for a slab geometry; we consider such an approximation acceptable, given the uncertainties in the geometry of active re-

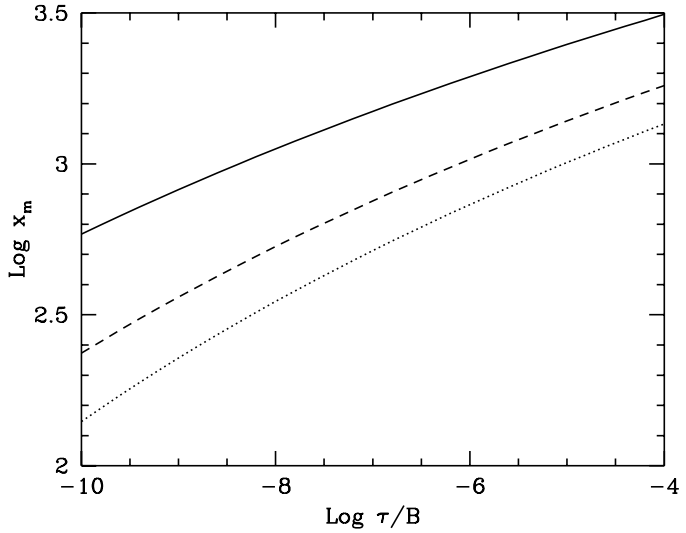

Figure 2. $x_{\rm m}$, which determines the self–absorption frequency is shown versus τ/B for three values of the electron temperature, namely $\theta = 0.6$ – solid line $\theta = 0.4$ – dashed line and $\theta = 0.2$ – dotted line.

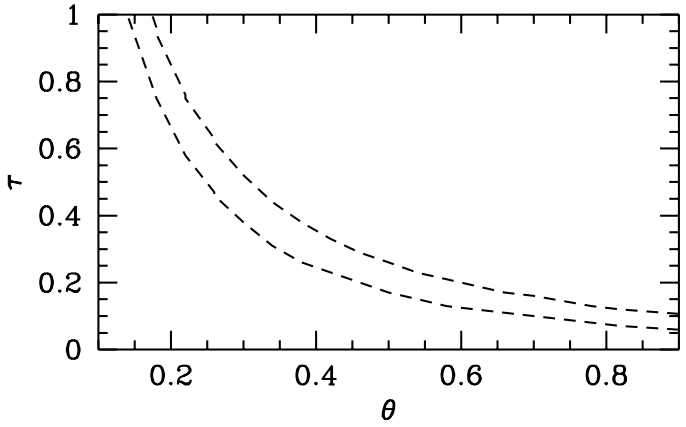

Figure 3. The area between the two dashed curves represents the region of parameter space for which combinations of θ and τ give $\alpha \simeq 1 \pm 0.1$.

gions and of dissipation through reconnection events (which could possibly take place in a sheet/shell geometry). By imposing $\alpha \sim 1$, we can therefore select the region of parameter space for τ and θ, shown in Fig. 3, for which to estimate the cooling rates.

The ratio in the case of GBHC (we take $M = 5\,{\rm M}_\odot$) and for $\theta = 0.4$ and $\tau = 0.3$ is given by

$$\begin{aligned}\frac{t_{\rm CS}}{t_{\rm iC}} &= 1.2\times10^{8}\frac{1-f}{f^{3/2}\eta^{1/2}}N^{3/2}\left(\frac{r_{\rm blob}}{r_{\rm cor}}\right)^{2}\frac{r_{\rm blob}\tau}{\Delta\theta^{6}x_{\rm m}^{3}}M^{1/2}\\ &\simeq 0.5\left(\frac{2}{\Delta}\right)\left(\frac{1-f}{0.5}\right)\left(\frac{0.5}{f}\right)^{3/2}\left(\frac{1}{\eta}\right)^{1/2}\\ &\times \left(\frac{N}{10}\right)^{3/2}\left(\frac{r_{\rm blob}}{1}\right)^{3}\left(\frac{50}{r_{\rm cor}}\right)^{2}\left(\frac{\tau}{0.3}\right)\\ &\times \left(\frac{0.4}{\theta}\right)^{6}\left(\frac{510}{x_{\rm m}}\right)^{3}\left(\frac{M}{5M_\odot}\right)^{1/2}. \end{aligned} \quad (9)$$

It is worth stressing that, given the observational dispersion in τ and θ, for the above calculation we have chosen intermediate values for these parameters (see Fig. 3). For sources which extend in the range of higher temperatures ($\theta \approx 0.7$) and lower values of the optical depth ($\tau = 0.1$) the ratio becomes of the order of 10^{-2}. In this same case, but for AGN with $M = 10^6\,{\rm M}_\odot$, it is given by $t_{\rm CS}/t_{\rm iC} \simeq 1$ where $x_{\rm m} = 626$ and $\Delta = 1.4$. This means that CS emission is very likely to be relevant in GBHC and may be important for AGN, depending on the values of the parameters.

2.2 Physical considerations

To estimate the size of the active regions we adopt the model developed by Galeev et al. (1979) and recently re–considered by Haardt et al. (1994) (see also Stern et al. 1995). There $r_{\rm blob} \sim z_0/\alpha_{\rm v}^{1/3}$, where from the geometrically thin accretion disk model (Shakura & Sunyaev 1973), the disk scale height z_0 is $\sim 9L/L_{\rm Edd}S(r)R_{\rm S}$, (where $S(r) = 1-(3/r)^{1/2}$) and $\alpha_{\rm v}$ is the viscosity parameter. In accordance with the Haardt et al. (1994) model, the total number of active regions at any time is chosen to be $N \sim 10$. This is consistent with the need to explain the amplitude of X-ray fluctuations on short timescales typically observed in AGN and GBHC.

Note that the importance of the CS emission depends strongly on the relative size of the active regions as compared to the disk extension $(r_{\rm blob}/r_{\rm cor})^2$. This ratio, however, is constrained by the fraction of soft photons intercepted and Compton scattered in these active regions (i.e. $Nr_{\rm blob}^2$ cannot exceed $r_{\rm cor}^2$). Actually this covering factor is estimated in some cases to be 50 per cent in sources where the UV/soft X–ray spectral component strongly dominates over the hard X–ray emission (however in most cases a covering factor significantly smaller than 50 per cent can be observationally inferred). The ratio of the two sizes has therefore to be at most $\lesssim 0.3$ if $N \sim 10$.

Under the assumptions adopted in eqn. (9) for the relative size of the two regions and the dissipation efficiency, the magnetic energy density (as calculated from eqn. (1)) largely exceeds both the radiation energy density, $U_{\rm rad}$, and the thermal particle (electron/positron) one, $\sim nm_{\rm e}c^2\theta$, which are of the same order. We note here that the powers released into magnetic field and disk radiation have been assumed to be of the order of $L_{\rm Edd}$. Sub-Eddington powers, i.e. $\eta \lesssim 1$, clearly influence the relative importance of the CS emission. However, as shown in eqn. 9, even for $\eta \sim 0.1$, the ratio of the cooling timescales varies only by a factor of 3.

The computation of the temporal evolution of the magnetic dissipation and consequent particle acceleration is beyond the aim of this paper. Here we can simply estimate the reconnection timescale for the stored magnetic field energy to be converted into particle energy. This can be written as $t_{\rm rec} \sim r_{\rm blob}R_{\rm s}/v_{\rm A}$, where the reconnection velocity is taken of the order of the Alfven speed $\sim c$ (Priest & Forbes 1986). Note that, unlike other authors, here we are not assuming a priori that the whole of the energy dissipated into the corona ($fL_{\rm Edd}$) is instantly released as radiation: the accretion energy is stored as magnetic energy in the active region and no efficiency is assumed in the conversion of the latter into radiation. It is then possible to estimate such efficiency by comparing the total energy stored in the

magnetic field with the energy radiated. Given that in our model the cooling timescale of the plasma is of the order of the reconnection timescale $t_{\rm rec}$, this corresponds to comparing $U_{\rm B}(4\pi/3)(r_{\rm blob}R_{\rm S})^3$ and $(r_{\rm blob}R_{\rm S}/c)L_{\rm blob}$, where $L_{\rm blob}$ is the total luminosity of an active region (all the radiative processes are taken into account). By computing $L_{\rm blob}$, we obtain a magnetic energy $\sim 90-200\times$ the radiated one, implying an extremely low efficiency in the energy conversion. The magnetic energy could then be efficiently converted if multiple reconnection events within the same active region occur.

To summarize this section, we find that CS emission from thermal electrons can play an important role if the active regions, or blobs, are localized and relatively small. Inverse Compton cooling is favoured instead in the case where the difference between the 'slab' and 'patchy' corona models becomes less extreme, either for a lower dissipation fraction f, or for higher covering factor of the active blobs. A similar trend is obtained for sub-Eddington accretion.

3 CYCLO–SYNCHROTRON EMISSION

We now consider the intensity of CS emission and its possible detectability, by comparing the predictions of the model with the spectral energy distributions of some AGN and GBHC.

The CS spectra for different parameters τ and θ are shown in Fig. 4a for a typical AGN. The plasma properties are again selected to produce a Comptonized spectrum (of the CS photons) with $\alpha\sim 1$. For comparison, a blackbody spectrum with energy density equivalent to the luminosity produced in the disk ($\eta(1-f)L_{\rm Edd}$) is also reproduced in the figure. Fig. 4a clearly shows that both $\nu_{\rm c}$ and the luminosity at this peak frequency depend primarily on θ (when the condition $\alpha\sim 1$ is satisfied). In particular if θ decreases, the luminosity follows it.

The analogous plot in Fig. 4b shows the dependence on different central masses, dimensions of the active regions and the dissipation fraction f. A decrease in mass implies a lower luminosity, but due to the increase in the equipartition magnetic field, leads to a higher self–absorption frequency. Clearly more coronal dissipation (higher f) gives rise to an enhancement in the frequency and luminosity of CS emission. The same effects are produced by reducing the size of the emitting regions.

3.1 Observational predictions

As discussed above, the peak of the CS emission is located in the IR–EUV band, strongly dependent on the black hole mass. At the same time the intensity of the emitted luminosity can be significant from an observational point of view. For this reason, we compare the predicted spectra with the spectral energy distribution (SED) of a few GBHC and radio-quiet AGN. The data (not simultaneous) have been collected from the literature in order to cover the broader possible spectral range. The CS and its relative Compton scattered component, have been self–consistently computed taking into account the relative importance of these processes with respect to the cooling by inverse Compton on the soft photons from the disk, as estimated above (see eqn. 9).

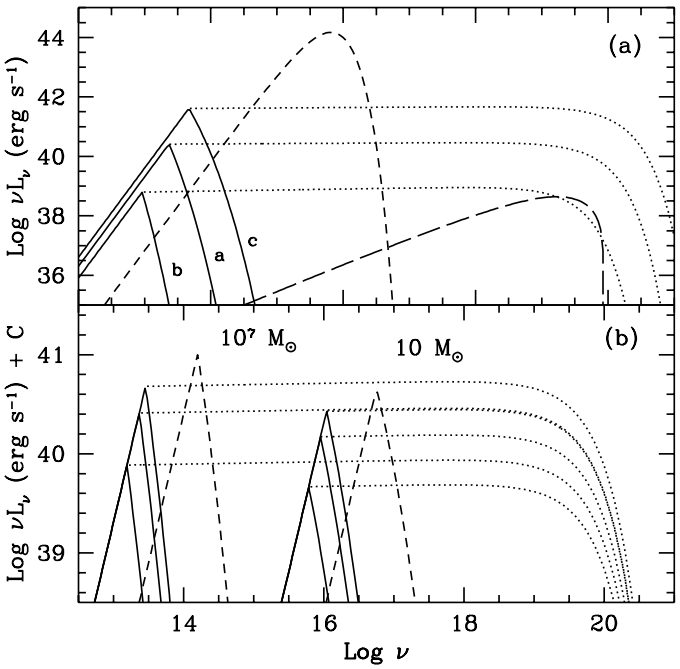

Figure 4. (a) Dependence of the CS spectral distribution (in νL_ν) on the physical parameters of the plasma, namely the temperature θ and optical depth τ. The spectra are estimated for a typical AGN, with $M=10^7M_\odot$, $f=0.5$ and $r_{\rm blob}=1$. The three solid curves represent the CS emission for $\theta=0.4$, $\tau=0.3$ (curve labelled a); $\theta=0.2$, $\tau=1$ (curve b); and $\theta=0.74$, $\tau=0.1$ (curve c). For comparison, the scattered inverse Compton (dotted lines) and bremsstrahlung (long-dash line) components are also reported for case a. The short-dash curve represents instead the blackbody emission from the disk. (b) The CS emission dependence on the black hole mass, fraction f of the accretion power magnetically dissipated and the dimension of the active regions. As labelled, the two sets of curves are computed for the cases $M=10^7M_\odot$ and $M=10M_\odot$ (where in the latter one the vertical axis has been displaced by a factor 10^4). For each set the three curves are computed for $f=0.2, 0.5, 0.8$, from bottom to top, respectively. Finally, the dashed lines refer to $r_{\rm blob}=0.1$. In all these cases $\theta=0.4$ and $\tau=0.3$.

Note that in the case of GBHC the radiation energy density in CS photons can exceed that of the disk.

The results of the comparison are presented in Figs. 5,6 for GBHC (GX 339–4, Cyg X–1, Nova Muscae and LMC X–3) and AGN (Seyfert 1 galaxies: NGC 5506, NGC 6814 and NGC 4051), respectively *. In the case of GHBC, the peak of the CS emission is in the EUV band, currently not observed, with the Compton–scattered CS flux which in some cases could exceed the X–ray flux level. The high energy tail of the CS emission can however be important at 0.1 keV. The CS emission itself can be comparable (within a factor of ~ 3 for GX 339–4) with the optical–UV measured fluxes and possibly contribute to the soft X–ray excess. This implies that the CS component could give rise to a detectable flux variability. Anti-correlation between optical and X-ray variations observed in GX 339-4 (Motch et al. 1983) can be consistent with the model, with a decrease in the field intensity after a reconnection event.

* Note that the masses adopted differ from those used in eqn. (9).

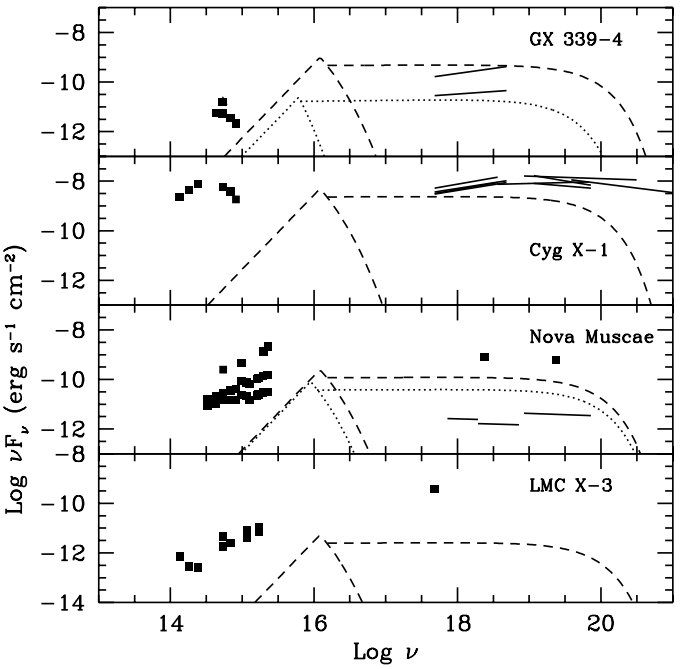

Figure 5. Comparison of the CS and inverse Compton emission with the SED of four GBHC, namely GX 339-4, Cygnus X-1, Nova Muscae and LMC X–3. The CS emission is estimated for a mass of $10M_\odot$, $f = 0.5$, $r_{\rm blob} = 1$, $\theta = 0.4$ and $\tau = 0.3$–dashed line. The dotted-line in GX 339-4 is calculated for $\theta = 0.15$ and $\tau = 1$ whereas the dotted-line in Nova Muscae is for $r_{\rm blob} = 0.8$. Data are from: Miyamoto et al. (1992), Makishima et al. (1986), Motch et al. (1983) (GX 339-4); Miyamoto et al. (1992), Salotti et al. (1992), Barr, White & Page (1985), Ling et al. (1983), Treves et al. (1980) (Cygnus X–1); King, Harrison & McNamara (1996), Gilfanov et al. (1993), Shrader & Gonzalez–Riestra (1993), Cheng et al. (1992) (Nova Muscae); Treves et al. (1990), Treves et al. (1988) (LMC X–3).

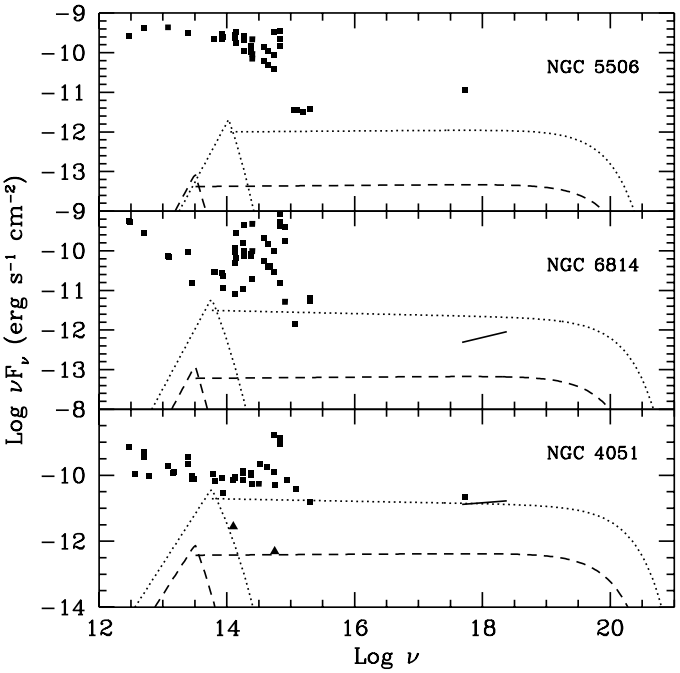

Figure 6. Analogous to Fig. 5, for the three bright Seyfert 1 galaxies NGC 5506, NGC 6814 and NGC 4051. The predicted emission is computed for $\theta = 0.4$, $\tau = 0.3$, $f = 0.8$, $r_{\rm blob} = 0.8$ and $M = 10^7 M_\odot$ –dashed lines. In NGC 6814 and NGC 4015 the dotted-line is determined with $\theta = 0.74$ and $\tau = 0.1$. In NGC 5506 the dotted curve is computed for a magnetic field $4\times B$. The two triangles in the SED of NGC 4051 indicate the variability limits reported by Done et al. (1990) (see the text). Data are from the following references: Kinney et al. (1993), White & Becker (1992), Fabbiano, Kim & Trinchieri (1992), De Vaucouleurs et al. (1991), Moshir et al. (1990), Soifer et al. (1989), McAlary et al. (1983), Glass (1981), Glass (1979) (NGC 5506); Reynolds (1997), Fabbiano, Kim & Trinchieri (1992), Celotti, Ghisellini & Fabian (1991), Moshir et al. (1990), McAlary & Rieke (1988), McAlary et al. (1983), Glass (1981), Glass (1979), Rieke (1978), Penston et al. (1974) (NGC 6814); Reynolds (1997), Fabbiano, Kim & Trinchieri (1992), De Vaucouleurs et al. (1991), Soifer et al. (1991), Gregory & Condon (1991), Moshir et al. (1990), Done et al. (1990), De Vaucouleurs & Longo (1988), Ward et al. (1987), Ficarra et al. (1985), Balzano & Weedman (1981), Lebofsky & Rieke (1979), McAlary et al. (1979), Rieke (1978), Rieke & Low (1972), Wisniewski & Kleinmann (1968) (NGC 4051).

In AGN, the CS spectral component is expected to contribute to the IR–near IR emission, with a flux which can be more than ~ 10 per cent of the observed one. Particularly interesting is the case of NGC 4051 for which constant IR and optical fluxes (within 1 per cent) have been observed simultaneously with a factor 2 fluctuation in the X-ray band (Done et al. 1990). In Fig. 6 we report these variable IR and optical flux constraints, which indeed set strong upper limits to any low energy radiation produced from the same population of electrons responsible for the X–ray emission. The detection of the CS component can be then a very powerful tool for investigating the physical conditions and the role of magnetic field in the inner corona of these sources. In particular, we stress that with an increase of only a factor of 4 in the field intensity, the predicted flux (and frequency) can increase to levels comparable with the data and the variability limits (e.g. the case of NGC 5506, see Fig. 6).

Note that here we used sets of parameters in the figures just as indicative predictions of the model. In particular, it is important to point out that even within the same source, the magnetic energy density is most likely to differ between the active regions.

We stress that the CS spectral component is expected to give rise to strong variability on short timescales as determined by the typical size of the active region ($\sim R_{\rm S}/c$) †, provided that the number of active regions N is small. Furthermore, the variability is predicted to be simultaneous to the X-ray one. A high degree of linear polarization, rapidly variable both in intensity and polarization angle, constitutes a further signature of the presence of thermal CS radiation.

We also stress that it is possible that the different states of individual GBHC (eg. Cyg X-1 and GX339-4) could be due to variations in the ratio and dominance of inverse Compton scattering of CS and external disk photons, e.g. to changes in B or $r_{\rm blob}$.

† Interestingly, some hints of small scale fast variations have been observed as intraday optical variability in several radio–loud sources and in some radio–quiet ones (e.g. Dultzin–Hacyan et al. 1992; Sagar, Gopal–Krishna & Wiita 1996)

4 SUMMARY

We have examined the role of CS emission in active regions, which are believed to be the loci of magnetic energy dissipation in the coronae of accretion disks. The particles, possibly energized through reconnection, are expected to have a thermal distribution, as also suggested by the observed high energy emission of radio-quiet AGN and GBHC.

The CS process can be an important cooling mechanism if the magnetic energy dissipation can occur in a much smaller volume than the soft thermal photon field which is distributed over the whole inner disk. Locally, the absorbed CS can then compete with Compton cooling on the photons produced by the disk. As a consequence of this, the effect of CS cooling on thermal electrons has to be considered in Comptonization models. We also note that self-absorbed CS emission can act as a rapid and efficient thermalizing mechanism for any initial electron distribution (Ghisellini, Guilbert & Svensson 1988).

Typical black hole masses and physical parameters of the thermal plasma are sufficient to produce observable radiative signatures, in both classes of sources, when ~ 50 per cent of the accreting power is dissipated into the corona. Even in the most unfavourable case of AGN, CS variable and polarized emission is predicted in the near IR band at a level above a few to tens of per cent. In GBHC the spectrum would be observable in the EUV band. Future monitoring in these bands with high temporal resolution, especially simultaneous with X-rays observations, can therefore provide crucial information on the physical conditions and main dissipation mechanisms in the very central regions of compact sources.

ACKNOWLEDGEMENTS

This research has made use of the NASA/IPAC extragalactic database (NED), which is operated by the Jet Propulsion Laboratory, California Institute of Technology, under contract with the National Aeronautic and Space Administration. We thank Dr. Juri Poutanen for useful comments. For financial support, we acknowledge PPARC and Trinity College, Cambridge (TDM), the Italian MURST (AC) and the Royal Society (ACF).

REFERENCES

Apparao K.M.V., 1984, A&A, 139, 377
Balzano V.A., Weedman D.W., 1981, ApJ, 243, 756
Barr P., White N.E., Page C.G., 1985, MNRAS, 216, 65p
Celotti A., Ghisellini G., Fabian A.C., 1991, MNRAS, 251, 529
Cheng F.H., Horne K., Panagia N., Shrader C.R., Gilmozzi R., Paresce F., Lund N., 1992, ApJ, 397, 664
De Vaucouleurs, A., Longo G., 1988, Catalogue of Visual and Infrared Photometry of Galaxies from 0.5 micron to 10 micron
De Vaucouleurs G., De Vaucouleurs A., Corwin J. H.G., Buta R.J., Paturel G., Fouque P., 1991, Third Reference Catalogue of Bright Galaxies, Version 3.9
Done C., Ward M.J., Fabian A.C., Kunieda H., Tsuruta S. Lawrence A., Smith M.G., Wamsteker W., 1990, MNRAS, 243, 713
Dultzin–Hacyan D., Schuster W.J., Parrao L., Pena J.H., Peniche R., Benitez E., Costero R., 1992, AJ, 103, 1769
Fabbiano G., Kim D.W., Trinchieri T., 1992, ApJS, 80, 531
Fabian A.C., Guilbert P.W., Motch C., Ricketts M., Ilovaisky S.A., Chevalier C., 1982, A&A, 111, l9
Ficarra A., Grueff G., Tomassetti T., 1985, A&As, 59, 255
Galeev A.A., Rosner R., Vaiana G.S., ApJ, 1979, 229, 318
Ghisellini G., Guilbert P.W., Svensson R., 1988, ApJ, 335, L5
Gilfanov M., et al., 1993, A&ASS, 97, 303
Glass I.S., 1979, MNRAS, 186, 29p
Glass I.S., 1981, MNRAS, 197, 1067
Gondek D., Zdziarski A.A., Johnson W.N., George I.M., McNaron-Brown K., Magdziarz P., Smith D., Gruber D.E., 1996, MNRAS, 282, 646
Gregory P. C., Condon J. J, 1991, ApjS, 75, 1011
Haardt F., Maraschi L., 1993, 413, 507
Haardt F., Maraschi L., Ghisellini G., 1994, ApJ, 432, L95
Ipser R.J., Price R.H., 1982, ApJ, 255, 654
King N.L., Harrison T.E., McNamara B.J., 1996, AJ, 111, 16
Kinney A.L., Bohlin R.C., Calzetti D., Panagia N., Wyse R.F., 1993, ApJS, 86, 5
Lebofsky M.J., Rieke G.H., 1979, ApJ, 229, 111
Ling J.C., Mahoney W.A., Wheaton W.A., Jacobson A.S., Kaluzienski L., 1983, ApJ, 275, 307
Mahadevan R., Narayan R., Yi I., 1996, ApJ, 465, 327
Makishima K., Maejima Y., Mitsuda K., Bradt H.V., Remillard R.A., Tuohy I.R., Hoshi R., Nakagawa M., 1086, ApJ, 308, 635
McAlary C.W., Rieke G.H., 1988, ApJ, 333, 1
McAlary, C.W., McLaren R. A., Crabtree D. R., 1979, ApJ, 234, 471
McAlary C.W., McLaren R.A., McGonegal R.J., Maza J., 1983, ApJS, 52, 341
Mihamoto S., Kitamoto S., Sayuri I., Negoro H., Terada K., 1992, ApJ, 391, L21
Moshir M., et al., 1990, Infrared Astronomical Satellite catalogs, The Faint Source Catalog, Version 2.0
Motch C., Ricketts M.J., Page C.G., Ilovaisky S.A., Chevalier C., 1983, A&A, 119, 171
Pacholczyk A.G., 1970, in Radio Astrophysics, Freeman (San Francisco)
Penston M.V., Penston M.J., Selmes R.A., Becklin E.E., Neugebauer G., 1974, MNRAS, 169, 357
Poutanen J., Svensson R., Stern B., 1997, Proceedings of 2nd INTEGRAL Workshop, San Malo, France, p.401
Priest E.R., Forbes T.G., 1986, J. Geophys. Res., 91, 5579
Reynolds C.S., 1997, MNRAS, in press
Rieke G.H., 1978, ApJ, 226, 550
Rieke G.H., Low F.J., 1972, ApJ, 176, L95
Sagar R., Gopal–Krishna, Wiita P.J., 1996, MNRAS, 281, 1267
Salotti L., et al., 1992, A&A, 253, 145
Shakura N.I., Sunyaev R.A., 1973, A&A, 24, 337
Shrader C.R., Gonzalez–Riestra R., 1993, A&A, 276, 373
Soifer B.T., Boehmer L., Neugebauer G., Sanders D.B., 1989, AJ, 98 ,766
Stern B.E., Poutanen J., Svensson R., Sikora M., Begelman M.C., 1995, ApJ, 449, L13
Takahara F., Tsuruta S., 1982, Prog. Theoret. Phys., 67, 485
Treves A., Belloni T., Bouchet P., Chiappetti L., Falomo R., Maraschi L., Tanzi E.G., 1988, ApJ, 335, 142
Treves A., et al., 1980, ApJ, 242, 1114
Treves A., et al., 1990, ApJ, 364, 266
Ward M., Elvis M., Fabbiano G., Carleton N.P., Willner S.P., Lawrence A., 1987, ApJ, 315, 74
White R.L., Becker R.H., 1992, ApJS, 98, 766
Wisniewski, W.Z., Kleinmann, D.E., 1968, AJ, 73, 866
Zdziarski A.A, 1986, ApJ, 289, 514
Zdziarski A.A., Fabian A.C., Nandra K., Celotti A., Rees M.J., Done C., Coppi P.S., Madejski G.M., 1994, MNRAS, 269, L55
Zdziarski A.A., Johnson W.N., Poutanen J., Magdziarz P., Giel-

rinski M., 1997, Proceedings of 2nd INTEGRAL Workshop,
San Malo, France, p. 373